

Automated Detection and Elimination of Periodic ECG Artifacts in EEG Using the Energy Interval Histogram Method

Hae-Jeong Park*, Do-Un Jeong, and Kwang-Suk Park, *Member, IEEE*

Abstract—An automated method for electrocardiogram (ECG)-artifact detection and elimination is proposed for application to a single-channel electroencephalogram (EEG) without a separate ECG channel for reference. The method is based on three characteristics of ECG artifacts: the spike-like property, the periodicity and the lack of correlation with the EEG. The method involves a two-step process: ECG artifact detection using the energy interval histogram (EIH) method and ECG artifact elimination using a modification of ensemble average subtraction. We applied a smoothed nonlinear energy operator to the contaminated EEG, which significantly emphasized the ECG artifacts compared with the background EEG. The EIH method was initially proposed to estimate the rate of false positives (FPs) and false negatives (FNs) that were necessary to determine the optimal threshold for the detection of the ECG artifact. As a postprocessing step, we used two types of threshold adjusting algorithms that were based on the periodicity of the ECG R-peaks. The technique was applied to four whole-night sleep EEG recordings from four subjects with severe obstructive sleep apnea syndrome, from which a total of 132 878 heartbeats were monitored over 31.8 h. We found that ECG artifacts were successfully detected and eliminated with $FP = 0.017$ and $FN = 0.074$ for the epochs where the elimination process is necessarily required.

Index Terms—Electrocardiogram (ECG) artifacts, energy interval histogram, ensemble average subtraction, nonlinear energy operator.

I. INTRODUCTION

THE need for ambulatory electroencephalographic monitoring has increased in both clinical practice and research, in areas such as sleep/wake state or epilepsy monitoring [1], [2]. However, long-term recordings are vulnerable to various artifacts. In particular, cardiac activity may have pronounced effects on the electroencephalogram (EEG) because of its relatively high electrical energy, especially upon the noncephalic reference recordings of EEG.

Manuscript received March 20, 2001; revised July 2, 2002. This work was the result of research activity of the Advanced Biometric Research Center supported by the Korea Science and Engineering Foundation. *Asterisk indicates corresponding author.*

*H.-J. Park was with the Advanced Biometric Research Center, Seoul National University College of Medicine, Seoul, Korea. He is now with the Department of Psychiatry, Harvard Medical School, Boston, MA 02115 USA.

D.-U. Jeong is with the Department of Psychiatry, Seoul National University College of Medicine and the Clinical Research Institute, Seoul National University Hospital, Seoul 110-744, Korea.

K.-S. Park is with the Department of Biomedical Engineering, Seoul National University College of Medicine, Seoul 110-744, Korea (e-mail: kspark@bmsil.snu.ac.kr).

Digital Object Identifier 10.1109/TBME.2002.805482

Algorithms have been proposed to eliminate electrocardiogram (ECG) artifacts from the EEG. Nakamura and Shibasaki [3] proposed an ECG artifact elimination algorithm, which we call the ensemble average subtraction (EAS) method, whereby ECG-contaminated EEG series are synchronously segmented with respect to the timing of consecutive ECG R-peaks. By subtracting the ensemble average across EEG segments from the contaminated EEG, the algorithm eliminates ECG artifacts. EAS is based on the strict assumptions of homogeneity across segments and Gaussian property of the EEG [3], [4].

Using a different concept, the independent component analysis (ICA) method was also applied to eliminate ECG artifacts using multichannel signals [7]. Previously, we adopted adaptive noise canceling theory [5] to eliminate such ECG artifacts using a reference ECG channel [6].

It should be noted that these algorithms use consecutive R-waves in a separate ECG channel as a reference, and therefore, cannot be applied when an ECG channel is not available. Several ambulatory monitoring systems used for studying sleep/wake states do not record ECG waveforms. Ambulatory sleep/wake recordings use a reduced number of essential channels, compared with the laboratory polysomnographic units. EEG, electrooculogram (EOG), and chin electromyogram (EMG) are necessary to assess the brain state, and nasal airflow, respiratory effort, oxygen saturation, and heart rate to monitor respiration and circulation. Recording heart rate is frequently preferred to recording the ECG waveform in order to reduce the data size when the ECG waveform is not a main concern. Therefore, a new method of eliminating ECG artifacts from the EEG is required when an ECG channel is unavailable.

In this paper, we propose an automated method for detecting ECG artifacts in a single-channel EEG, and a method for eliminating them.

II. MATERIALS AND METHODS

The proposed method for elimination of ECG artifacts involves a two-step process: 1) ECG artifact detection using the energy interval histogram (EIH) method, and 2) ECG artifact elimination using a modification of the EAS method. In this paper, we will focus primarily on the ECG artifact detection method and then briefly deal with ECG artifact elimination.

A. Detection Procedure: Energy Interval Histogram Method

The smoothed nonlinear energy operator (SNEO) was used to emphasize the ECG R-waves that corrupt the pure EEG signals,

and the EIH technique was developed to estimate the optimal threshold using threshold-adjusting algorithms.

Step 1: Emphasizing the ECG Artifacts Using SNEO: The SNEO [8], which uses the Teager–Kaiser Energy Operator [9]–[11], is regarded as an efficient tool for detecting spike-like signals because of its sensitivity to instantaneous changes in frequency-dependent energy.

For a discrete-time series, the nonlinear energy operator Ψ and SNEO can be defined as follows [8]:

$$\Psi[x(n)] = x^2(n) - x(n+1)x(n-1) \quad (1)$$

$$\Psi_s[x(n)] = \Psi[x(n)] \otimes w(n) \quad (2)$$

where \otimes is the convolution operator and $w(n)$ is a smoothing window function. SNEO is dependent on the square of both the amplitude and the frequency of the signal, and shows high energy for a high-frequency spike. For a linear combination of source signal x and spike artifact s , i.e., $y(n) = x(n) + s(n)$, where x and s are uncorrelated, the expected energy applying SNEO to y is expressed by (3) (for detailed derivation, refer to [8])

$$sy(n) = \Psi_s[y(n)] = \Psi_s[x(n)] + \Psi_s[s(n)]. \quad (3)$$

For spike-dominant positions, $\Psi_s[x(n)] = \Psi_s[s(n)]$, $sy(n) \approx \Psi_s[s(n)]$ while for nonspike positions, $\Psi_s[s(n)] \approx 0$, $sy(n) \approx \Psi_s[x(n)]$. Using this property of SNEO, the problem of detecting an ECG spike in the presence of the EEG background is reduced to finding an appropriate threshold T that separates the spike regions from background signal regions by the equation $sy(n) > T$.

Mukhopadhyay and Ray [8], defined the threshold of SNEO as the mean energy multiplied by a scaling factor C as follows:

$$T = C \frac{1}{N} \sum_{n=1}^N \Psi_s[y(n)]. \quad (4)$$

The scaling factor C is initially determined by experiment and used as a constant thereafter. This threshold method cannot be adapted to nonstationary situations where the spike energy of the ECG artifacts in the EEG is variable and no precise knowledge is available on the energy distributions of the spikes and the background activities. Therefore, we developed a new automated threshold-selection and threshold-adjusting algorithm, as described in the following steps.

Step 2: EIH for Estimating the Optimal Threshold: For detection problems in general, the optimal threshold is determined to minimize false negatives (FNs) while maintaining false positives (FPs) within a reasonably low limit [12]. In the present application, FPs are more crucial than FNs, because the subsequent EAS procedure can be severely disrupted by false alarms. Therefore, an optimal threshold should be chosen to minimize FPs at a reasonable FN level. However, it is not easy to derive the FP and FN rates and the corresponding optimal threshold mathematically, because we have no exact knowledge on the *a priori* probability density functions of the EEG and ECG artifact energy. Therefore, we used a heuristic approach to estimate FP and FN rates.

After detecting peaks from the smoothed signal energy (sy), we applied a series of thresholds (T) to these peaks (denoted as

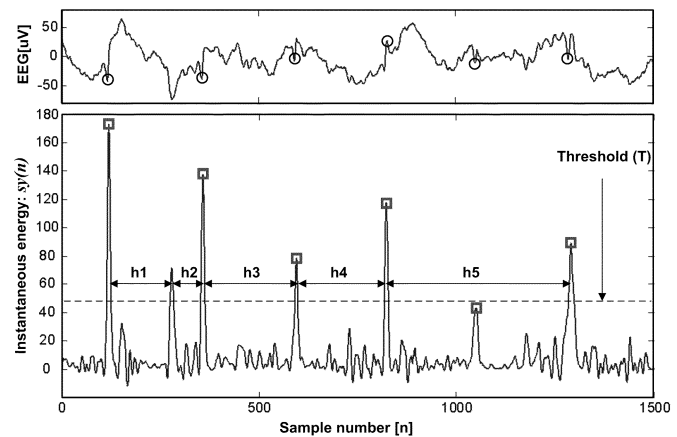


Fig. 1. An illustration of energy intervals. Intervals between peaks were calculated from the instantaneous energy distribution $sy(n)$ (lower figure) emphasized using the SNEO of contaminated EEG (upper figure). The circle marks (o) in the upper figure and square marks (□) in the lower figure indicate the real R-peak positions on the ECG. Only peaks above the threshold T were used for interval calculation. Neighboring peak intervals h3 and h4 fall within normal heart beat interval range (I_{HB}) while h1, h2 fall within half the normal heart beat interval range ($I_{HB/2}$), and h5 falls within twice the normal heart beat interval range (I_{2HB}) at a threshold T .

Psy), whereby T was varied from the maximal value of Psy to its minimal value. Only the peaks higher than the resulting threshold value of T were used to calculate a histogram of peak intervals. We called this histogram the EIH and have denoted it as $H(T)$, i.e., as a function of the threshold T . An example of energy intervals is illustrated in Fig. 1, where an ECG-contaminated EEG and its SNEO energy are also displayed. The energy peaks above the threshold T form a series of intervals (i.e., h1–h5).

Histogram bins of $H(T)$ were divided into three ranges: normal heart beat interval range (I_{HB}), twice the normal heart beat interval range (I_{2HB}), and half the normal heart beat interval range ($I_{HB/2}$). These ranges are defined with respect to the expected normal heart beat range (I_{EHB}) as follows:

$$\begin{aligned} I_{HB/2} &\equiv \{I \mid I < \frac{1}{2} I_{EHB}\} \\ I_{HB} &\equiv \{I \mid \frac{3}{4} I_{EHB} \leq I < \frac{5}{4} I_{EHB}\} \\ I_{2HB} &\equiv \{I \mid \frac{3}{2} I_{EHB} \leq I\}. \end{aligned} \quad (5)$$

In case of multiepoch signals, I_{EHB} was initially given with an arbitrary normal range value for the first epoch and was estimated for subsequent epochs by the mean heart beat interval of the previous epochs.

In Fig. 1, the intervals h3 and h4 fall within I_{HB} whereas h1 and h2 fall within $I_{HB/2}$, and h5 falls within I_{2HB} , at the threshold T .

The numbers of intervals that fall into the aforementioned three ranges are denoted as $H_{HB/2}(T)$, $H_{HB}(T)$, and $H_{2HB}(T)$. At a high value of T , most intervals of the peaks fall in I_{2HB} . As T decreases, the intervals fall more into I_{HB} and $H_{HB}(T)$ increases while $H_{2HB}(T)$ decreases. As T is reduced further toward the minimal value, most intervals fall within $I_{HB/2}$ and $H_{HB/2}(T)$ is maximized. For practical purposes, we counted the number of intervals directly within the three ranges of (5) instead of calculating the intervals in smaller-sized bins. Fig. 2 illustrates the course of EIH according to the threshold, at (a)

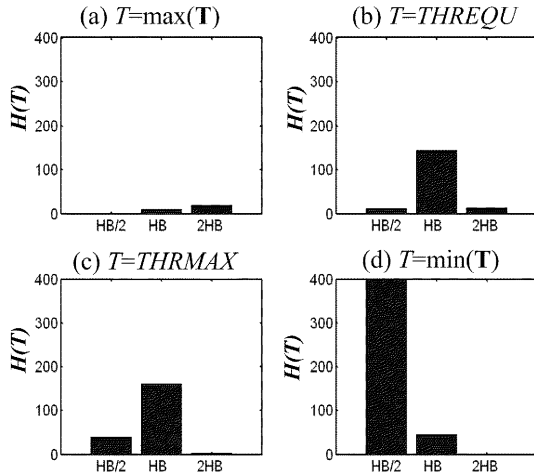


Fig. 2. An illustration of the energy interval histogram $H(T)$ according to the thresholds: (a) $T = \max(\mathbf{T})$, (b) $T = \text{THREQU}$, (c) $T = \text{THRMAX}$, and (d) $T = \min(\mathbf{T})$. As the threshold T decreases, $H_{\text{HB}/2}$ increases while $H_{2\text{HB}}$ decreases. At THREQU , the relative number of intervals within $I_{\text{HB}/2}$ is the same as that within $I_{2\text{HB}}$, i.e., $H_{\text{HB}/2}(\text{THREQU}) = H_{2\text{HB}}(\text{THREQU})$. THRMAX is the threshold that maximizes rH_{HB} , i.e., H_{HB} divided by the total number of intervals.

$T = \max(\mathbf{T})$, (b) $T = \text{THREQU}$, (c) $T = \text{THRMAX}$, and (d) $T = \min(\mathbf{T})$. In this figure, $\min(\mathbf{T}) < \text{THRMAX} < \text{THREQU} < \max(\mathbf{T})$.

The relative histograms $rH_{\text{HB}/2}(T)$, $rH_{\text{HB}}(T)$, and $rH_{2\text{HB}}(T)$ indicate the ratios of $H_{\text{HB}/2}(T)$, $H_{\text{HB}}(T)$, and $H_{2\text{HB}}(T)$ with respect to the number of total intervals within all three intervals of (5), which is denoted by $H_{\text{TOT}}(T) = H_{\text{HB}/2}(T) + H_{\text{HB}}(T) + H_{2\text{HB}}(T)$. $rH_{2\text{HB}}$ is highly correlated with the number of missed peaks (an estimate of FN, abbreviated as eFN) and $rH_{\text{HB}/2}$ is highly correlated with the number of false alarms (an estimate of FP, abbreviated eFP). rH_{HB} implies true positives (eTP). Using the estimated values for $rH_{\text{HB}/2}(T)$, $rH_{\text{HB}}(T)$, and $rH_{2\text{HB}}(T)$, we considered four criteria for selecting the optimal threshold

$$\begin{aligned} \text{THREQU} &\equiv \arg\{rH_{\text{HB}/2}(T) = rH_{2\text{HB}}(T)\} \\ \text{THROPT} &\equiv \arg\{\min[rH_{\text{HB}/2}(T)], rH_{2\text{HB}}(T) < rH_{\text{Lim}}\} \\ \text{THRMAX} &\equiv \arg\{\max[rH_{\text{HB}}(T)]\}. \end{aligned} \quad (6)$$

THREQU represents the threshold at which the false alarm rate eFP and the miss rate eFN have the same value. THROPT is a threshold chosen to minimize eFP while maintaining eFN within a reasonable limit rH_{Lim} (0.1 in this study). THRMAX is the threshold that maximizes the eTP. Fig. 3 shows the EIHF function derived using the procedures previously described and shows the relative number of intervals according to the threshold.

Step 3: Postprocessing of Detection: STEP 3-1: Reducing false alarms using the next-spike selection algorithm.

Since random high-frequency noise frequently disturbed the detection of periodic ECG spikes, we reduced these false alarms using the nonperiodic characteristics of random noise. When multiple peaks were detected within 1.5 times the mean heart-

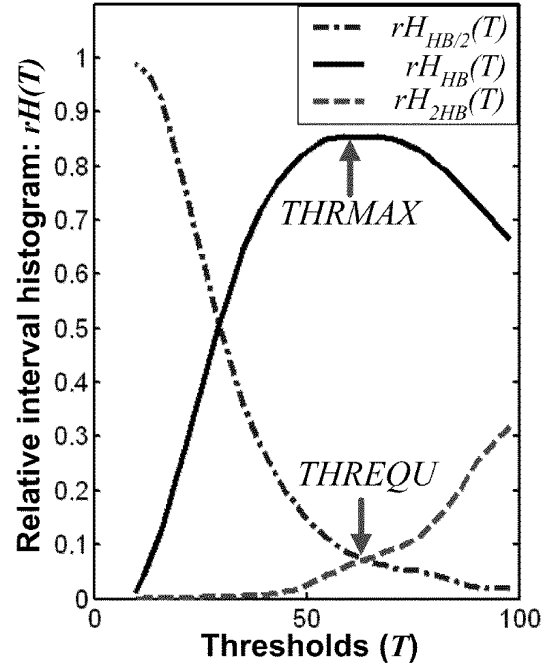


Fig. 3. A relative energy interval histogram $rH(T)$ as a function of threshold T . $rH(T)$ are functions of the relative number of intervals that fall within predetermined ranges at the threshold T . The dark solid line is $rH_{\text{HB}}(T)$, the dash-dotted line is $rH_{\text{HB}/2}(T)$, and the dashed line is $rH_{2\text{HB}}(T)$. These functions were derived by normalizing $H_{\text{HB}/2}(T)$, $H_{\text{HB}}(T)$, and $H_{2\text{HB}}(T)$ with respect to $H_{\text{TOT}}(T)$.

beat interval ($1.5 \times I_{\text{EHB}}$) from the reference spike, the most likely position of the following spike was considered to be the position delayed by I_{EHB} from the reference spike, due to the periodic characteristic of ECG spike trains. The peak nearest the expected position was selected as a new reference. With the exception of this selected peak, other peaks within $0.2 \times I_{\text{EHB}}$ of the reference peak were regarded as false alarms. When no spikes were found within $1.5 \times I_{\text{EHB}}$ from the reference, a new reference was selected using an interval mask ranging from two to four times I_{EHB} after the current peak with a mask gap of $2I_{\Delta}$ as follows: $c \times I_{\text{EHB}} - I_{\Delta} < I < c \times I_{\text{EHB}} + I_{\Delta}$, $c = 2, 3, 4$. By shifting this mask to consecutive peaks and counting the number of peaks that fall within the mask, the peak with the highest coincident number was selected as a new reference on the assumption of periodicity.

Fig. 4 illustrates this procedure. The peaks detected by thresholding are marked with plus signs (+). Within $1.5 \times I_{\text{EHB}}$ from the reference $i_{\text{sy}}(\text{ref}_1)$, the most likely ECG-peak position is represented by the peak that is closest to the expected peak position, i.e., $i_{\text{sy}}(\text{ref}_1) + I_{\text{EHB}}$. In Fig. 4, I_3 shows the nearest interval to I_{EHB} and $i_{\text{sy}}(\text{ref}_1) + I_3$ is selected as a new spike reference $i_{\text{sy}}(\text{ref}_2)$. $i_{\text{sy}}(\text{ref}_3)$ can be calculated using the same procedure with the reference being $i_{\text{sy}}(\text{ref}_2)$.

STEP 3-2: Reducing misses using the threshold-adjusting algorithm.

In order to redetect missed spikes, we applied a threshold-adjusting technique around the expected spike regions with a threshold window. This window has a triangular shape with a minimal peak value equal to a constant multiplied by the

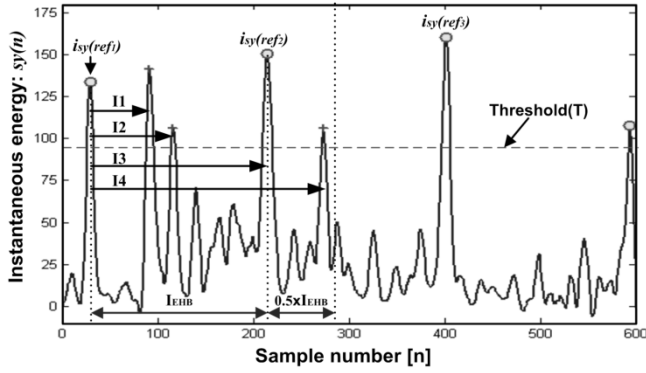


Fig. 4. An illustration of the next-spike selection algorithm. In the energy plot of ECG-contaminated EEG, all intervals from the reference $i_{sy}(\text{ref}_1)$ within $1.5 \times I_{\text{EHB}}$ (I_1 , I_2 , I_3 , and I_4) are displayed with arrows. The plus (+) and circle (o) signed peaks are spike candidates higher than the threshold; the circles indicate true spikes. Within $1.5 \times I_{\text{EHB}}$ from the reference $i_{sy}(\text{ref}_1)$, the most probable position is the peak nearest the expected peak position, i.e., $i_{sy}(\text{ref}_1) + I_{\text{EHB}}$. Of the intervals, the peak delayed by I_3 is nearest the expected heart beat peak and is regarded as a new spike. I_1 and I_2 are considered to be false alarms and rejected. The peak located at $i_{sy}(\text{ref}_1) + I_4$ will be recalculated with a new reference $i_{sy}(\text{ref}_2)$ and will be rejected as a false alarm.

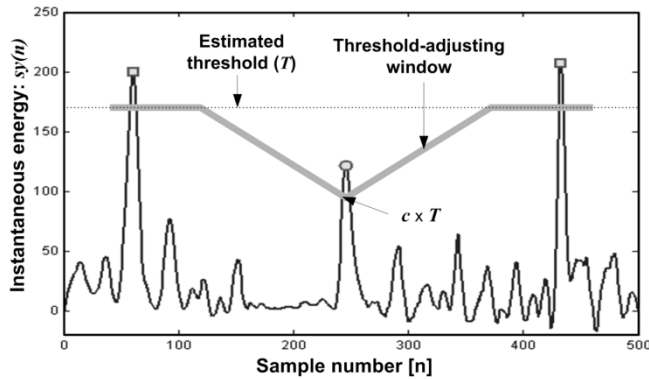


Fig. 5. The threshold-adjusting algorithm. When a spike is missed, a triangular window with a minimum of $c \times T$ at the mid-way position between spikes is applied in an effort to re-detect the missed spike. The square marks (□) indicate peaks detected by the thresholding method initially, while the circle mark (o) indicates a missed spike, to be re-detected by lowering the threshold.

threshold $T(c \times T)$ in the expected region. This is shown in Fig. 5.

STEP 3-3: Reducing false alarms by removing points neighboring the expected beats.

During STEP 3-2, a lowered threshold may cause the re-detection of artifacts and increase the number of FPs. Therefore, re-application of STEP 3-1 is required to reduce these extra FPs.

Fig. 6 is an illustration of the result of each detection step, and was obtained by plotting heart beat intervals versus the detected heartbeats. Beat intervals much shorter than the mean beat interval (I_{EHB}) can be regarded as false alarms while beat intervals two or three times longer than I_{EHB} can be regarded as indicating misses. After thresholding spike energies in STEP 2, false alarms and misses occurred with $\text{FP} = 0.08$ and $\text{FN} = 0.1$ in this example [Fig. 6(a)]. The first postprocessing step STEP 3-1 removed the false alarms of STEP 2 using the next-spike selection algorithm [Fig. 6(b)]. STEP 3-2 re-detected the misses using the threshold-adjusting algorithm [Fig. 6(c)], using a tri-

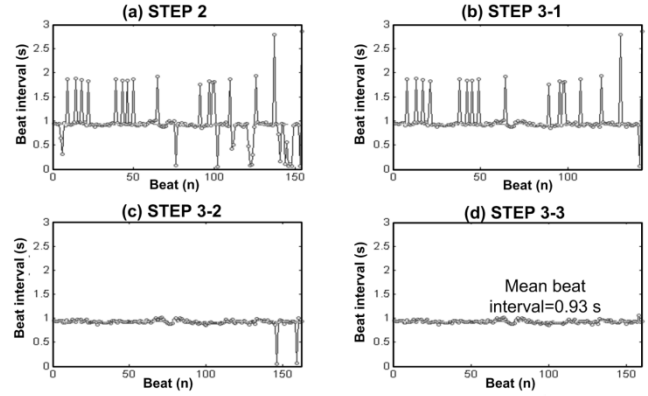


Fig. 6. Results at four detection steps. The estimated beats and the intervals between neighboring beats are plotted on the x and y axes, respectively. (a) Shows peaks thresholded by an optimal threshold which is derived from EIH in STEP 2. (b) Shows the resultant peaks after application of the next-spike selection algorithm, which reduced false alarms in STEP 3-1. (c) Result of the threshold-adjusting algorithm for reducing misses in STEP 3-2. The final result of STEP 3-3, in which the (d) next-spike selection algorithm reduces the false alarms caused by STEP 3-2.

angle-weighted threshold window when the heart beat intervals were longer than two or three times I_{EHB} . STEP 3-3 reduced the false alarms generated by STEP 3-2 to give a final FP of 0.006 and a final FN of 0.006 [Fig. 6(d)].

B. Elimination of ECG Artifacts: EAS

We adopted EAS [3] with a small modification. For ECG-contaminated EEGs, $y(n) = x(n) + s(n)$, where $x(n)$ is the original EEG and $s(n)$ is the ECG spike, the R-peaks of the reference ECG can be used as triggering points for averaging. All EEG signals were segmented onto the time range between 200 ms prior to the current triggering point and 200 ms prior to the next triggering point. By averaging these segments, an estimate of the ECG artifact waveform can be derived by the following equation:

$$\begin{aligned} \frac{1}{M} \sum_{i=1}^M y_i(n) &= \frac{1}{M} \sum_{i=1}^M \{x_i(n) + s_i(n)\} \\ &= \frac{1}{M} \sum_{i=1}^M x_i(n) + \frac{1}{M} \sum_{i=1}^M s_i(n) \end{aligned} \quad (7)$$

where M is the number of the segments and i denotes the segment index. On the assumption that the EEG has a zero-mean Gaussian distribution, the first term of the equation can be reduced to zero, leaving only the second term. The remainder [i.e., $\hat{s}(n) = 1/M \sum_{i=1}^M s_i(n)$] is an ensemble average and indicates an estimation of the ECG artifact. By subtracting this ensemble average from the contaminated EEG (y_i), the original EEG waveform (x_i) can be estimated using $\hat{x}_i(n) = y_i(n) - \hat{s}(n)$. For the nonstationary case when the ECG waveform varies with time or there are multiepoch events, the previously calculated ECG ensemble average can be added, with a weight factor λ , in a new averaging process as shown by the following equation:

$$\hat{s}_{e+1}(n) = \lambda \hat{s}_e(n) + (1 - \lambda) / M \sum_{i=1}^M y_i(n). \quad (8)$$

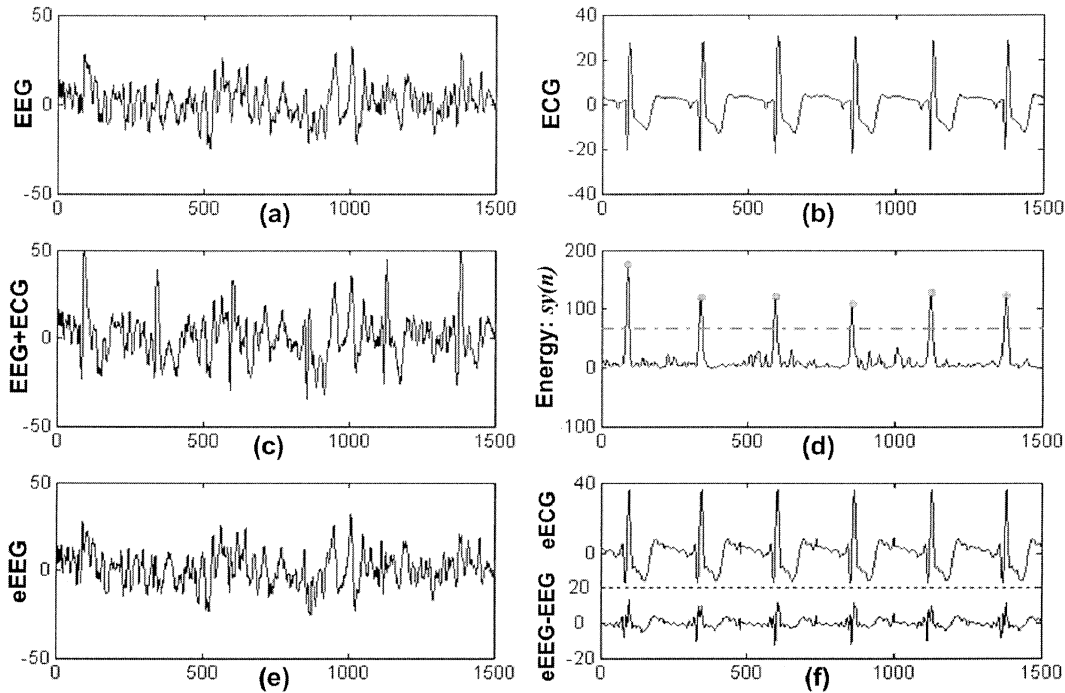


Fig. 7. Detection and elimination of simulated ECG-artifacts.

This ensemble average across EEG segments is computed, assuming that only ECG artifacts and no true cerebral activity are time-locked to the R-wave in the recorded EEG. In this paper, the bias errors between the exact spike peaks and the detected peaks cannot be disregarded, and therefore, the EAS algorithm of Nakamura and Shibasaki [3] above was modified. Before subtracting the averaged ECG component from the EEG, we realigned the averaged ECG artifact segment to the real EEG segment with a time delay. The time delay τ was derived to make the cross-correlation between both segments maximal and can be described as follows:

$$\tau = \arg \left\{ \max_t \left\{ \frac{1}{M - 2L - 1} \sum_{n=-L}^L [y_i(n-t) \times \hat{s}(n)], \right. \right. \\ \left. \left. \text{for } -L < t < L \right\} \right\} \quad (9)$$

where M is the length of the averaged ECG waveform and L is the maximum time shift around the peak. The resultant EEG is calculated using $\hat{x}_i(n) = y_i(n) - \hat{s}(n + \tau)$.

Fig. 7 illustrates the complete process used for ECG artifact detection and elimination in the simulated signals. Artifact-free EEG signals [Fig. 7(a)] and the time-synchronized ECG artifacts [Fig. 7(b)] were added to generate the simulated EEG + ECG [Fig. 7(c)]. Fig. 7(d) shows the energy of the EEG + ECG derived from the SNEO. The estimated EEG (eEEG) using our algorithm is shown in Fig. 7(e). Fig. 7(f) shows the estimated ECG artifacts derived by subtracting the eEEG from the simulated EEG + ECG (top) and the difference between the original EEG and estimated EEG (bottom).

III. EVALUATIONS AND RESULTS

A. Evaluation Sets

In order to evaluate the performance of the artifact detection and elimination algorithm, we acquired six 8-h EEGs (C3-A2 or O2-A1) during sleep from one normal subject and five subjects with obstructive sleep apnea syndrome (OSAS). One OSAS recording was used for determining the optimal detection parameters, one normal recording was used for evaluating ECG elimination performance, and the other four recordings were used for evaluating the overall performance of our method.

All recordings of the OSAS subjects contained ECG artifacts in the EEG, but no ECG artifacts were present in the normal recording. In all cases, the ECG was recorded simultaneously with the EEG, as a reference. Both ECG and EEG signals were sampled at a frequency of 250 Hz. R-peaks of the reference ECG, detected using a general R-peak detection algorithm [13] were used as a target for evaluating the detection performance.

B. Performance Indexes

Spike-to-Background Signal Energy Ratio (SBR): SBR was defined to be a function of mean spike energy normalized with respect to the background signal energy. In practice, we defined SBR as the ratio of the mean energy of the spike region to that of the background signal as follows:

$$\text{SBR} = \frac{\sum_{k=1}^{N_k} \left(\frac{1}{N_S^{(k)}} \sum_{n=1}^{N_S^{(k)}} SE^{(k)}(n) \right)}{\sum_{k=1}^{N_k} \left(\frac{1}{N_B^{(k)}} \sum_{n=1}^{N_B^{(k)}} BE^{(k)}(n) \right)} \quad (10)$$

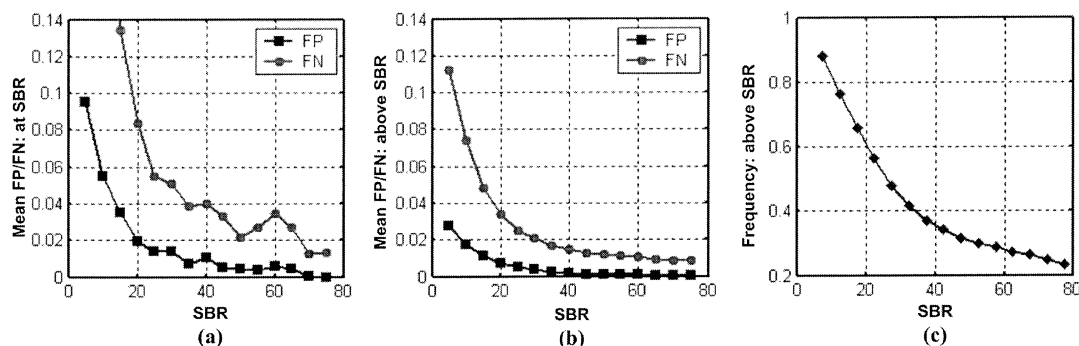


Fig. 8. Detection performance versus SBR in OSAS recordings (total 3814 epochs and 132 878 heartbeats during 3814×30 s). (a) Illustrates mean FP and FN in the epochs of the given SBR. (b) Mean FP and FN in the epochs having higher SBR than the given SBR. (c) Relative number of epochs having higher SBR than the given SBR. SBRs higher than 20, whereby FP and FN reached 0.02 and 0.1, accounted for 60% of the total epochs.

where $SE^{(k)}(n)$ and $BE^{(k)}(n)$ indicate the instantaneous signal energy of the spike region and of the nonspike region in the k th segment, with segment sizes of $N_S^{(k)}$ and $N_B^{(k)}$, respectively. Each segment is composed of samples located around the R-peak and N_k is the number of total segments in the epoch.

FN Ratio : FN was defined as the ratio of the number of missed spikes to the number of actual spikes.

FP Ratio: FP was defined as the ratio of the number of false alarm spikes to the number of actual spikes.

In the cases of both FP and FN, the R-peaks of the ECG reference were regarded as actual spikes.

C. Performance Evaluation

Bartlett, Hamming, and rectangular windows were tested as a smoothing window for the SNEO, and a rectangular window of length of seven samples was found to produce the best results in emphasizing spike-to-signal ratio maximally.

The Detection Performance According to Detection Steps: We optimized the detection parameters by applying the current method to ECG-contaminated EEG samples (1068 heartbeats with mean heart rate 71.2 beats/min within a duration of 15 min) derived from the EEG recording of one OSAS subject, including sleep stage 1, stage 2, REM, and wakefulness state. In order to evaluate the validity of threshold selection by EIH at STEP2, we compared the estimated thresholds (i.e., THREQU, THROPT, and THRMAX) with an experimentally determined optimal threshold, which was chosen to minimize FP and FN using real ECG R-peak references. The FP and FN of the ECG-referenced results were 0.08 and 0.09, respectively, and these values were equal to the maximal performance that can be achieved by the thresholding method. The high correlation ($r = 0.99$) between the ECG-referenced, the experimental optimal threshold and one type of estimated threshold (THREQU) derived by EIH supported the use of EIH for estimating the optimal threshold.

Though FP and FN at STEP2 were dependent on the threshold type, no significant differences were evident after postprocessing. We selected THREQU as an optimally estimated threshold because THREQU requires less calculation time than the other thresholds. However, in particular situations when THREQU could not be obtained, we used the

average value of the other threshold types, i.e., THROPT and THRMAX.

STEP3-1 reduced FP at the cost of a slight increase in FN. STEP3-2 then decreased FN while STEP 3-3 readjusted the FP. Due to the postprocessing algorithms, FP and FN were reduced to 0.008 from 0.0763 and to 0.008 from 0.0109, respectively, using THREQU.

The Elimination Performance: The performance of elimination using EAS was evaluated using simulated signals that were generated by adding weighted ECG spike trains to the artifact-free normal EEG. The mean power error between the original signals and the ECG-eliminated signals, normalized to the original signal power, was 10%. The elimination procedure reduced the SBR of the contaminated EEG from 25.3 to 3.1.

Application to the OSAS Recordings: Four OSAS recordings were used to evaluate the overall performance of the algorithm. The mean sleep time of each subject was 7.94 h (i.e., on the average 953.5 epochs of 30 s each) and the total number of heartbeats was 132 878 during a total period of 31.8 h with a mean heart rate of 69.7 beats/min. The mean respiratory disturbance index (RDI) was 49.9 (counts/h), indicating severe OSAS. Sleep stages were scored according to Rechtschaffen and Kales' sleep staging criteria [14] by a sleep expert. The total epoch numbers of stage 1, stage 2, REM, and wakefulness were 530, 2244, 555, and 485, respectively. Mean FP was 0.0424 and FN was 0.1504 for total epochs.

Fig. 8 illustrates the relationship between SBR and the performance indices FP and FN. Fig. 8(a) shows the mean FP and FN in the epochs with the given SBR, and Fig. 8(b) shows the mean FP and FN in the epochs having SBR higher than the given SBR. Fig. 8(c) indicates the relative number, i.e., frequency, of epochs having SBR higher than the given SBR. As is shown in Fig. 8(a), an SBR value higher than 20 was required for FP and FN to reach 0.02 and 0.1, respectively. Epochs having an SBR higher than 20 account for 60% of the total epochs in Fig. 8(c). Inspection of epochs with SBR around 20 indicated that the EEG signals contained other types of artifact-bursts such as EMG, which made it difficult to identify some ECG artifacts. For epochs with an SBR below ten, ECG artifacts could not be discriminated easily due to other types of artifacts present, or due to a relatively small ECG effect on the EEG. Therefore, ECG artifact elimination in these epochs ($SBR < 10$) was not thought to be

TABLE I
PERFORMANCE ACCORDING TO THE SLEEP STAGES IN OSAS RECORDINGS

	Stage1	Stage2	REM	Wakeful	Mean
SBRr	70.1	49.3	123.6	19.0	59.2
SBRe	5.9	5.9	12.1	3.4	6.4
<i>FP</i>					
<i>Total</i>	0.042	0.044	0.018	0.064	0.042
<i>SBR > 10</i>	0.021	0.018	0.010	0.019	0.017
<i>FN</i>					
<i>Total</i>	0.133	0.163	0.066	0.209	0.150
<i>SBR > 10</i>	0.081	0.081	0.040	0.079	0.074

*SBRr : spike-to-background ratio of energy of original signals

*SBRe : spike-to-background ratio of energy after ECG-elimination

necessary. These epochs accounted for as much as 20% of the epochs and it would make sense to exclude these epochs in the performance evaluation. The detection performance at epochs of $SBR > 10$ was $FP = 0.017$ and $FN = 0.074$ in Fig. 8(b). For epochs of $SBR > 20$, which was regarded as the boundary of obviousness for ECG artifacts by visual inspection, the algorithm achieved $FP = 0.007$ and $FN = 0.034$ [Fig. 8(b)].

In Table I, results of the performance are listed according to sleep stages. Wakefulness states showed the lowest SBR and the highest FP and FN. This result can be explained by the fact that in the sleep of OSAS, a wakefulness state usually follows apneic events with deep exhalation, which is associated with severe movement and muscle artifacts. During REM stages, the SBR was at its highest and the number of FPs and FNs at their lowest. Upon applying the algorithm, the SBR decreased from 59.2 to 6.5 on the average, which confirms the efficiency of the algorithm.

IV. DISCUSSION

We propose an ECG artifact detection and elimination method for EEG without the need for an additional ECG channel. The method is based on the following three characteristics of ECG artifacts: that the ECG R-peak occurs as a spike, that the ECG R-peak has periodicity, and that the ECG is uncorrelated with the EEG.

The SNEO showed excellent performance in emphasizing spike components by a simple calculation. The EIH method utilized ECG periodicity when estimating FP and FN to determine an optimal threshold. Moreover, the EIH method allowed the experimentally obtained optimal threshold to be approximated.

It should be noted that the detection performance with the experimental optimal threshold derived by using an ECG reference was much lower than that obtained by using the procedures of EIH method. This indicates the intrinsic limitation associated with the fixed thresholding method, due to the presence of the changing environment caused by the background EEG. In some ECG spike regions, the original EEG activity may be of the opposite phase to the ECG activity and, thus, may degrade the spike energy. Conversely, the original EEG activity may be in-phase, which would increase the ECG spike energy. These situations explain the diverse instantaneous energy distribution of ECG spikes. In addition, SNEO is relatively sensitive to high-frequency noise, such as EMG signals that are frequently present in EEG signals. Therefore, additional

algorithmic adjustment is required to overcome the degradation of ECG detection caused by the various environments. In order to decrease the number of misses and false alarms, two threshold-adjusting procedures were applied. One procedure involved rejecting spikes of shorter interspike duration than the expected heart beat interval. The other procedure redetected missed events by adjusting the threshold in the expected peak region using ECG periodicity information. These adjusting steps increased the detection performance significantly.

The application to OSAS data produced satisfactory results. According to the results obtained, the performance of our algorithm was mainly dependent on SBR. In the low-SBR cases, ECG artifacts tend to be immersed in other artifacts or are not easily distinguished from the EEG and in such cases, there is no need to apply the ECG-artifact elimination algorithm.

We did not evaluate the performance of the method systematically according to heart rate variability and ECG waveform changes. However, recordings of OSAS involving various sleep stages can be considered to present a somehow extreme case of heart-rate variability and ECG waveform changes which may be exacerbated in the presence of several types of heart disorders. In the case of OSAS signals where the standard deviation of heart beat intervals was extended to almost 25 % of the mean heart beat interval, we found no significant correlation between the standard deviation of heart beat intervals and FP or FN within the same SBR range. Therefore, we believe that the algorithm has enough redundancy, provided the cardiac activity maintains periodicity within the normal ranges.

ECG waveform variability, due to, for example, amplitude variation of R-peaks, may not severely disrupt the detection performance, if such variability remains within normal limits, considering that the ECG waveform change is equivalent to a change in the background EEG in the sense of additive energy. However, the artifact-elimination performance of the EAS algorithm is believed to be dependent on the ECG waveform variability even if the algorithm uses the adaptive averaging method of (8).

We believe that the elimination algorithm is worth examining further, even though this is not the main concern of this paper. Some intrinsic limitations were found in the EAS algorithm of [3], which was based on the assumption that the beat-to-beat QRS waveform is constant and every beat is averaged with a triggering reference of time-locked R peaks. In order to satisfy the time-locking assumption, the bias between the estimated R-peaks and the accurate position of R-peaks should be minimized. However, in the non-ECG reference case, the bias may be unavoidable, and, therefore, we used a temporal realignment technique, using template matching in order to reduce the bias effect.

One merit of the proposed method is its excellent detection performance in terms of real contaminated signals. In epochs where the elimination process is thought to be necessary ($SBR > 10$), the average FP was 0.017 and the average FN was 0.074 (Table I), which is an acceptable result for clinical signals. The other merit of the method is that it uses only one channel of contaminated EEG. The simplicity of the algorithm is another merit for successful implementation in practical real-time situations. If this algorithm is applied to multichannel

EEGs, and if the time synchronization information between channels were used, we would expect increased detection and elimination performance in the low-SBR situation.

This paper proposes an efficient method for detecting and eliminating periodic artifacts, and we believe that it has the potential for more general application in systems that involve periodic or semiperiodic spike artifacts.

REFERENCES

- [1] R. Broughton, J. Fleming, and J. Fleetham, "Home assessment of sleep disorders by portable monitoring," *J. Clin. Neurophys.*, vol. 13, no. 4, pp. 272–284, 1996.
- [2] B. Van Sweden, M. Koenderink, G. Windau, M. Van de Bor, F. Van Bel, J. G. Van Dijk, and A. Wauquier, "Long-term EEG monitoring in the early premature: Developmental and chronobiological aspects," *Electroencephalogr. Clin. Neurophys.*, vol. 79, pp. 94–100, 1991.
- [3] M. Nakamura and H. Shibasaki, "Elimination of EKG artifacts from EEG records: A new method of noncephalic referential EEG recording," *Electroencephalogr. Clin. Neurophys.*, vol. 66, pp. 89–92, 1987.
- [4] J. L. Kenemans, P. C. M. Molenaar, and M. N. Verbaten, "Models for estimation and removal of artifacts in biological signals," in *Digital Biosignal Processing, Techniques in the Behavioral and Neural Sciences*, R. Weitkunat, Ed. Amsterdam, The Netherlands: Elsevier, 1991, vol. 5, ch. 9.
- [5] B. Widrow and S. D. Stearns, "Adaptive interference canceling," in *Adaptive Signal Processing*. Upper Saddle River, NJ: Prentice-Hall, 1985, ch. 12, pp. 302–367.
- [6] H. Park, J. Han, D. Jeong, and K. Park, "A study on the elimination of the ECG artifact in the polysomnographic EEG and EOG using AR model," in *Proc. 20th Ann. Int. Conf. IEEE Engineering Medicine Biology Soc.*, vol. 3, 1998, pp. 1632–1635.
- [7] R. Everson and S. J. Roberts, "Independent component analysis," in *Artificial Neural Networks in Biomedicine*, P. J. G. Lisboa, E. C. Ifeachor, and P. S. Szczepaniak, Eds. New York: Springer-Verlag, 2000, ch. 12.
- [8] S. Mukhopadhyay and G. C. Ray, "A new interpretation of nonlinear energy operator and its efficacy in spike detection," *IEEE Trans. Biomed. Eng.*, vol. 45, pp. 180–187, Feb. 1998.
- [9] J. F. Kaiser, "On a simple algorithm to calculate the energy of a signal," in *Proc. IEEE Int. Conf. Acoustic Speech Signal Processing*, Albuquerque, NM, 1990, pp. 381–384.
- [10] R. B. Dunn, T. F. Quatieri, and J. F. Kaiser, "Detection of transient signals using energy operator," in *Proc. IEEE Int. Conf. Acoustic Speech Signal Processing*, vol. 3, 1993, pp. 145–148.
- [11] P. Maragos, J. F. Kaiser, and T. F. Quatieri, "On amplitude and frequency demodulation using energy operators," *IEEE Trans. Signal Processing*, vol. 41, pp. 1532–1550, Apr. 1993.
- [12] H. L. Van Trees, *Detection, Estimation, and Modulation Theory: Part I*. New York: Wiley, 1968.
- [13] O. Pahlm and L. Sornmo, "Software QRS detection in ambulatory monitoring," *Med. Biol. Eng. Comput.*, pp. 289–297, 1984.

- [14] A. Rechtschaffen and A. Kales, Eds., "A manual of standardized terminology," in *Techniques and Scoring System for Sleep Stages of Human Subjects*. Los Angeles, CA: BIS/BRI, UCLA, 1968.



Hae-Jeong Park was born in KyungNam, Korea, in 1970. He received the B.S. degree in electrical engineering and the M.S. and Ph.D. degrees in biomedical engineering, from Seoul National University, Seoul, Korea, in 1993, 1995, and 2000, respectively.

He is currently working as a Research Fellow at the Clinical Neuroscience Division, Laboratory of Neuroscience, Boston VA Health Care System—Brockton Division, Department of Psychiatry and Surgical Planning Laboratory, MRI Division, Department of Radiology, Brigham and

Women's Hospital, Harvard Medical School, Boston, MA. His research interests include biomedical signal processing, biomedical image analysis, and neuroimaging.



Do-Un Jeong received the M.D. and Ph.D. degrees from the Seoul National University, Seoul, Korea, in 1976 and 1988, respectively.

He is currently a Professor of Psychiatry at the Seoul National University and a Researcher at the Clinical Research Institute of the Seoul National University Hospital and at the Neuroscience Research Institute of the Seoul National University. He was trained in sleep medicine and physiology and is a Diplomat of the American Board of Sleep Medicine. He is the Director of Division of Sleep

Studies at the Seoul National University Hospital and doing research in sleep disorders, chronobiology, and signal processing.

Dr. Jeong is a Fellow of the American Academy of Sleep Medicine and is currently President of the Korean Academy of Sleep Medicine.



Kwang-Suk Park was born in Seoul, Korea, in 1957. He received the B.S., M.S., and Ph.D. degrees in electronic engineering, especially for biomedical engineering, from the Seoul National University, Seoul, Korea, in 1980, 1983, and 1985 respectively.

He is currently the Professor and Chairman of the Department of Biomedical Engineering, Seoul National University College of Medicine. His research interests include biomedical signal processing, biomedical image analysis, and medical instrumentation.